INTERNATIONAL JOURNAL FOR NUMERICAL METHODS IN ENGINEERING
Int. J. Numer. Meth. Engng 2008; **73**:1413–1433
Published online 9 July 2007 in Wiley InterScience (www.interscience.wiley.com). DOI: 10.1002/nme.2124

Time-dependent fibre reorientation of transversely isotropic continua—Finite element formulation and consistent linearization

G. Himpel[1], A. Menzel[2], E. Kuhl[3] and P. Steinmann[1,*,†]

[1]*Chair of Applied Mechanics, Department of Mechanical and Process Engineering, University of Kaiserslautern, Kaiserslautern, Germany*
[2]*Institute of Mechanics and Control Engineering, Department of Mechanical Engineering, University of Siegen, Siegen, Germany*
[3]*Department of Mechanical Engineering, Stanford University, Palo Alto, CA, U.S.A.*

SUMMARY

Transverse isotropy is realized by one characteristic direction—for instance, the fibre direction in fibre-reinforced materials. Commonly, the characteristic direction is assumed to be constant, but in some cases—for instance, in the constitutive description of biological tissues, liquid crystals, grain orientations within polycrystalline materials or piezoelectric materials, as well as in optimization processes—it proves reasonable to consider reorienting fibre directions. Various fields can be assumed to be the driving forces for the reorientation process, for instance, mechanical, electric or magnetic fields. In this work, we restrict ourselves to reorientation processes in hyper-elastic materials driven by principal stretches.

The main contribution of this paper is the algorithmic implementation of the reorientation process into a finite element framework. Therefore, an implicit exponential update of the characteristic direction is applied by using the Rodriguez formula to express the exponential term. The non-linear equations on the local and on the global level are solved by means of the Newton–Raphson scheme. Accordingly, the local update of the characteristic direction and the global update of the deformation field are consistently linearized, yielding the corresponding tangent moduli. Through implementation into a finite element code and some representative numerical simulations, the fundamental characteristics of the model are illustrated.

Received 10 November 2006; Revised 21 May 2007; Accepted 21 May 2007

KEY WORDS: reorientation; transverse isotropy; fibre-reinforced materials

1. INTRODUCTION

Transverse isotropic materials, i.e. materials with one characteristic direction, can be found in various fields of our daily life. In many cases the characteristic direction is fixed in the matrix

*Correspondence to: P. Steinmann, Chair of Applied Mechanics, Department of Mechanical and Process Engineering, University of Kaiserslautern, D-67663 Kaiserslautern, Germany.
†E-mail: ps@rhrk.uni-kl.de

material, but in living materials, particularly, the characteristic direction changes due to changes in their environments. These changes can be either smooth and continuous, for instance, in biological materials, or discontinuous, as in piezoelectric materials. One example for smoothly reorienting transversely isotropic materials is biological soft tissue such as muscle tissue, cartilage tissue or our skin, where the characteristic directions, for instance, the muscle fibres or the collagen fibres, adapt their orientations to their mechanical loading environment. So far it is not clearly investigated which are the driving forces for the reorientation process in biomaterials. Some authors advocate that principal stretches are the biological stimulus in soft tissues, see for instance, Driessen *et al*. [1–4], Kuhl *et al*. [5] and Menzel [6]. In Hariton *et al*. [7], stresses are chosen to drive the reorientation process. For a combined model of growth and reorientation, the reader is referred to Imatani and Maugin [8] and Menzel [9]. Another example for reorienting transversely isotropic materials are liquid crystals, i.e. liquids with a crystalline structure. The physical condition of these materials is between the solid and the fluid phase. As is common in transversely isotropic materials, the characteristic direction of a liquid crystal is described by a position-dependent director. The most common application of liquid crystals is in liquid crystal displays, but they are also a central component of biological systems, such as in myelin, DNS, protein and cell membranes. Further, liquid crystals can be found in polymers, thermometers, pressure sensors, etc. For a broad outline of liquid crystals, the reader is referred to the book of Collings [10]. Driving forces for the reorientation process in liquid crystalline materials, among others, are contact with other materials, electric or magnetic fields, see Ericksen [11].

To give another example on anisotropic reorienting materials, recall that piezoceramics can be poled by displacements or electric fields, so that the polarization direction characterizes transversely isotropic material behaviour. Thereby, two fundamentally different piezoelectric effects can be observed. The direct piezoelectric effect characterizes charging of the material caused by applied stresses as, for instance, used in sensors. In actuators, the inverse piezoelectric effect is exploited, which means that an applied electric field induces mechanical strains. For a general survey on piezoelectric materials, we refer to Kamlah [12] and Smith [13]. Due to mechanical or electrical loading, switching of the polarization direction may be induced, where a difference between ferroelastic switching and ferroelectric switching is made. Ferroelastic switching refers to reorientation of domains under purely mechanical loading and ferroelectric switching refers to reorientation under electric loading, see, e.g. Schröder and Romanowski [14] and Arockiarajan *et al*. [15–17] and the references cited therein.

In general, reorientation phenomena can be observed in various polycrystalline materials, of which metals are a classical example. Apart from texture evolution, for instance, related to the constitutive behaviour within the individual grain, such grains might themselves reorient according to the overall loading conditions. In this regard, a thermodynamically consistent and stress-driven framework has, among others, been proposed by Johansson *et al*. [18]. For a general survey, the reader is referred to the contributions in Kocks *et al*. [19].

Furthermore, simulations including reorienting characteristic directions can be used in the context of optimization problems for composites, for instance, reinforced concrete in civil engineering or carbon fibre-reinforced materials in motor sports, yachting, aircraft or wind engine construction, see for example, Pedersen [20]. For optimization problems, typically, principal stresses or strains are assumed as driving forces.

It can be shown that for anisotropic elasticity the free energy reaches a critical state for commutating stresses and strains, see Vianello [21, 22] and Sgarra and Vianello [23]. Since the stresses and strains are coaxial if the characteristic direction is aligned with the principal stretch direction,

DOI: 10.1002/nme

we postulate reorientation along the maximum principal strain direction. Furthermore, in this contribution, we restrict ourselves to hyper-elastic formats for the stress tensor. The major intention of this paper is the derivation of a robust and efficient algorithmic formulation and its consistent linearization within a finite element framework. In this context, we assume as an additional material property a rotation of the characteristic direction, where in drilling rotations are excluded. Even though we will restrict ourselves to studying a specific constitutive model, the general algorithmic formulation can be applied to a wide range of applications. To be specific, the consistent linearization related to a reorienting fibre direction embedded into an iterative finite element context will be useful for various types of adaptive materials as indicated above.

The paper is organized as follows: The constitutive framework for transversely isotropic materials is summarized in Section 2. This includes the essential kinematic equations for finite deformations as well as the constitutive description of transverse isotropy. In Section 3, essential equations describing the reorientation process are derived. Firstly, the evolution in time of a line element according to a rigid body motion is considered, later on to describe the evolution of the characteristic direction driven by principal stretches. Section 4 contains the consistent linearization of the material model, including an algorithmic update scheme for the characteristic direction as well as the incremental tangent modulus. In the last section, we discuss the material model by means of numerical examples. Firstly, the material behaviour is demonstrated by a simple tension test before we apply the theory to a homogeneous and an inhomogeneous boundary value problem. The paper closes with a short conclusion in Section 6.

2. CONSTITUTIVE FRAMEWORK

In this section, we summarize in brief the essential kinematics for the non-linear deformation problem, as well as the constitutive equations for transversely isotropic hyper-elasticity. For a detailed overview on non-linear continuum mechanics, we refer to the monographs by Chadwick [24] and Holzapfel [25].

2.1. Essential kinematics

Let $\mathbf{X}$ and $\mathbf{x}$ denote the placements of a particle in the material and the spatial configurations $\mathscr{B}_0$ and $\mathscr{B}_t$ at times t_0 and t, respectively, and $\boldsymbol{\varphi}$ the appropriate non-linear deformation map

$$\mathbf{x} = \boldsymbol{\varphi}(\mathbf{X}, t) \tag{1}$$

The corresponding deformation gradient

$$\mathbf{F} = \nabla_{\mathbf{X}} \boldsymbol{\varphi}(\mathbf{X}, t) \tag{2}$$

describes the tangent map from the material tangent space $T_{\mathbf{X}}\mathscr{B}_0$ to the spatial tangent space $T_{\mathbf{X}}\mathscr{B}_t$ and $J := \det \mathbf{F} > 0$ is the Jacobian. As a deformation measure, we introduce the right Cauchy–Green tensor in the material configuration

$$\mathbf{C} = \mathbf{F}^{\mathrm{t}} \cdot \mathbf{F} = \sum_{I=1}^{3} \lambda_I^C \mathbf{n}_I^C \otimes \mathbf{n}_I^C \tag{3}$$

DOI: 10.1002/nme

with $\mathbf{n}_I^C$ denoting the principal stretch direction associated with the principal stretch λ_I^C, whereby, in this contribution we sort the principal stretches such that the index I increases with increasing principal stretch, namely

$$\mathbf{n}_I^C \cdot \mathbf{n}_J^C = \delta_{IJ}, \quad \lambda_1^C \leqslant \lambda_2^C \leqslant \lambda_3^C \tag{4}$$

To describe the evolution in time of the spatial line element with respect to the spatial line element itself

$$\mathrm{d}\dot{\mathbf{x}} = \frac{\partial \dot{\mathbf{x}}}{\partial \mathbf{x}} \cdot \mathrm{d}\mathbf{x} = \nabla_{\mathbf{x}} \mathbf{v} \cdot \mathrm{d}\mathbf{x} \tag{5}$$

the spatial velocity gradient can be introduced as

$$\mathbf{l} = \nabla_{\mathbf{x}} \mathbf{v} = \dot{\mathbf{F}} \cdot \mathbf{F}^{-1} \tag{6}$$

with $\{\dot{\bullet}\} = \partial_t \{\bullet\}|_{\mathbf{X}}$ characterizing the material time derivative of a quantity $\{\bullet\}$ and $\mathbf{v} = \dot{\mathbf{x}}$ being the spatial velocity.

2.2. Transversely isotropic hyper-elasticity

For the representation of transverse isotropy, it is common practice to introduce the characteristic direction $\mathbf{n}^A$ in the material configuration or rather the sign-independent structural tensor $\mathbf{A}$, whereby in this contribution the characteristic direction is assumed to be a non-constant, reorienting unit vector

$$\mathbf{A} = \mathbf{n}^A \otimes \mathbf{n}^A \quad \text{with } \mathbf{n}^A \cdot \mathbf{n}^A = 1 \quad \text{and} \quad \mathbf{n}^A \neq \text{const} \tag{7}$$

The characteristic direction describes, for instance, the fibre direction in a fibre-reinforced material or the collagen fibres in the arterial wall. Thus, the evolution of the characteristic direction must be orthogonal to the characteristic direction itself

$$\frac{\mathrm{d}}{\mathrm{d}t}(\mathbf{n}^A \cdot \mathbf{n}^A) = 0 \implies \dot{\mathbf{n}}^A \cdot \mathbf{n}^A = 0 \tag{8}$$

Following the notation of Schönflies, see Borchardt-Ott [26], transverse isotropy is characterized by the symmetry group $D_{\infty h} := \{\mathbf{Q} \in \mathcal{O}(3) | \mathbf{Q} \cdot \mathbf{A} \cdot \mathbf{Q}^{\mathrm{t}} = \mathbf{A}\}$. The evolution equation describing the reorientation process is introduced in Section 3.

To describe the characteristic material response, constitutive equations must be defined. In this contribution, we restrict ourselves to the modelling of hyper-elasticity, which requires the definition of a free energy function ψ_0, depending on the deformation gradient $\mathbf{F}$. To satisfy the invariance under superposed rigid body motions, the dependency of ψ_0 on the deformation gradient is commonly realized by a dependency on the right Cauchy–Green tensor $\mathbf{C}$. Since the free energy of an anisotropic material depends, in general, on the orientation of the material, an exclusive dependence of ψ_0 on $\mathbf{C}$ would lead to an anisotropic free energy function, i.e. for transverse isotropy

$$\psi_0(\mathbf{C}) = \psi_0(\mathbf{Q} \cdot \mathbf{C} \cdot \mathbf{Q}^{\mathrm{t}}) \quad \forall \mathbf{Q} \in D_{\infty h} \tag{9}$$

whereby the second-order tensor $\mathbf{Q}$ is restricted to be a member of the transversely isotropic symmetry group $D_{\infty h}$. For an isotropic representation of anisotropic tensor functions, based on

DOI: 10.1002/nme

the works of Lokhin and Sedov [27] and Boehler [28], we extend the tensor function isotropically by means of structural tensors. This leads to the following isotropic representation of the free energy function for transverse isotropy

$$\psi_0 = \psi_0(\mathbf{C}, \mathbf{A}) = \psi_0(\mathbf{Q} \cdot \mathbf{C} \cdot \mathbf{Q}^{\mathrm{t}}, \mathbf{Q} \cdot \mathbf{A} \cdot \mathbf{Q}^{\mathrm{t}}) \quad \forall \mathbf{Q} \in \mathcal{O}(3) \tag{10}$$

with $\mathbf{Q}$ now being allowed to be any member of the orthogonal group $\mathcal{O}(3)$. The dependency on the right Cauchy–Green tensor and the structural tensor is realized by invariants, for instance, the basic invariants $I_{i=1,2,3} = \mathrm{tr}(\mathbf{C}^i)$ and the mixed invariants $I_{i=4,5} = \mathrm{tr}(\mathbf{C}^{i-3} \cdot \mathbf{A})$

$$\psi_0 = \psi_0(\mathbf{C}, \mathbf{A}) = \psi_0(I_1, I_2, I_3, I_4, I_5) \tag{11}$$

see Spencer [29] and Schröder [30]. Insertion of the free energy function (11) into the Clausius–Planck inequality

$$\mathscr{D}_0 = \tfrac{1}{2}\, \mathbf{S} : \dot{\mathbf{C}} - \dot{\psi}_0 - \theta \mathscr{S}_0 \geqslant 0 \tag{12}$$

together with the definition of the Piola–Kirchhoff stresses as work conjugate quantity to the right Cauchy–Green tensor

$$\mathbf{S} := 2 \frac{\partial \psi_0}{\partial \mathbf{C}} \tag{13}$$

yields the reduced dissipation inequality

$$\mathscr{D}_0^{\mathrm{red}} = -\frac{\partial \psi_0}{\partial \mathbf{A}} : \dot{\mathbf{A}} - \theta \mathscr{S}_0 \geqslant 0 \tag{14}$$

The standard form of the dissipation inequality $\mathscr{D}_0 = \frac{1}{2}\mathbf{S} : \dot{\mathbf{C}} - \dot{\psi}_0 \geqslant 0$ might here be violated by the evolution of the characteristic direction. As described in Garikipati *et al*. [31] for the description of remodelling, processes that may stiffen the material, chemical or thermal processes must be included to satisfy thermodynamical consistency. Thus, as is common in the theory of open systems, we introduced the extra entropy term $\mathscr{S}_0$ in Equations (12) and (14) to capture such effects, which, apart from these two instances, are not explicitly addressed in this article. For a detailed outline, the reader is referred to the textbook of Holzapfel [25] in the context of closed systems and to the works of Epstein and Maugin [32], Kuhl and Steinmann [33, 34], Himpel [35] and Menzel [6] in the context of open systems. In this work, we confine ourselves to representations with respect to the material setting. For a direct formulation of hyper-elasticity in terms of spatial arguments, see Menzel and Steinmann [36] and Menzel [9].

3. EVOLUTION EQUATION

In this section, the reorientation of the characteristic direction is described by means of an evolution equation. Even though a particular format is chosen, the general numerical approach can be applied to different types of adaptation processes.

3.1. Evolution in time of a line element

Each second-order tensor $\mathbf{T} = \mathbf{T}^{\mathrm{sym}} + \mathbf{T}^{\mathrm{skw}}$ can be decomposed into a symmetric part $\mathbf{T}^{\mathrm{sym}} = \mathrm{sym}(\mathbf{T}) = \frac{1}{2}[\mathbf{T} + \mathbf{T}^{\mathrm{t}}]$ and a skew symmetric part $\mathbf{T}^{\mathrm{skw}} = \mathrm{skew}(\mathbf{T}) = \frac{1}{2}[\mathbf{T} - \mathbf{T}^{\mathrm{t}}]$. Since any skew symmetric

DOI: 10.1002/nme

tensor is completely characterized by three scalar values, it can also be described by its axial vector $\mathbf{t} = -\frac{1}{2}\mathbf{T}^{\mathrm{skw}} : \boldsymbol{\varepsilon}$, with $\boldsymbol{\varepsilon}$ denoting the third-order permutation tensor. The action of the skew tensor applied to any vector $\mathbf{a} \in \mathbb{R}^3$ is identical to the cross-product of the corresponding axial vector and $\mathbf{a}$, i.e. $\mathbf{T}^{\mathrm{skw}} \cdot \mathbf{a} = \mathbf{t} \times \mathbf{a}$.

The symmetric—skew symmetric decomposition of the velocity gradient in (6) yields

$$\mathbf{l} = \mathbf{d} + \mathbf{w} \tag{15}$$

with the rate of deformation tensor and the spin tensor

$$\mathbf{d} = \mathrm{sym}(\mathbf{l}) = \tfrac{1}{2}[\mathbf{l} + \mathbf{l}^{\mathrm{t}}] \quad \text{and} \quad \mathbf{w} = \mathrm{skew}(\mathbf{l}) = \tfrac{1}{2}[\mathbf{l} - \mathbf{l}^{\mathrm{t}}] \tag{16}$$

respectively. The spin tensor can also be represented by its axial vector $\boldsymbol{\omega}$ and describes the rate of rotation contained in the deformation map. For rigid body motions $\mathbf{x}(\mathbf{X}, t) = \mathbf{c}(t) + \mathbf{R}(t) \cdot \mathbf{X}$, where $\mathbf{R}$ is the proper orthogonal rotation tensor, the spatial velocity gradient becomes

$$\mathbf{l} = \dot{\mathbf{R}} \cdot \mathbf{R}^{\mathrm{t}} \quad \forall \mathbf{R} \in \mathscr{SO}(3) \tag{17}$$

which is a skew symmetric tensor field. Thus, for a rigid body motion, the rate of deformation tensor vanishes and the spin tensor is equal to the spatial velocity gradient:

$$\mathbf{d} = \mathbf{0} \quad \text{and} \quad \mathbf{w} = \mathbf{l} = \dot{\mathbf{R}} \cdot \mathbf{R}^{\mathrm{t}} \tag{18}$$

so that the variation of the line element in (5) with respect to time reduces to a pure rotation:

$$\mathrm{d}\dot{\mathbf{x}} = \mathbf{w} \cdot \mathrm{d}\mathbf{x} = \boldsymbol{\omega} \times \mathrm{d}\mathbf{x} \tag{19}$$

3.2. Kinematics-based reorientation

As depicted in Figure 1(a), the evolution of the characteristic direction $\dot{\mathbf{n}}^A$ can be represented as a rotation about the axis $\boldsymbol{\omega}^A$. Thus, analogous to Equation (19), the variation of the characteristic direction in time becomes

$$\dot{\mathbf{n}}^A = \boldsymbol{\omega}^A \times \mathbf{n}^A \tag{20}$$

wherein the angular velocity $\boldsymbol{\omega}^A$ must be specified in more detail. Recall that the orthogonality condition in (8) is *a priori* satisfied.

For linear and finite elasticity, it has been shown that a critical state of the free energy can be reached if the strain and stress tensors are coaxial, see for instance, Cowin [37], Vianello [21, 22] and Sgarra and Vianello [23, 38]. In isotropic materials this condition is *a priori* satisfied, however, in anisotropic materials this is not satisfied *a priori*. Insertion of the invariant-based version of the free energy function $(11)_2$ into the general definition of the Piola–Kirchhoff stresses (13) and application of the chain rule yields the Piola–Kirchhoff stresses

$$\mathbf{S} = 2\sum_{i=1}^{5} \frac{\partial \psi_0}{\partial I_i} \frac{\partial I_i}{\partial \mathbf{C}} = S_1\mathbf{I} + S_2\mathbf{C} + S_3\mathbf{C}^2 + S_4\mathbf{A} + 2S_5[\mathbf{A} \cdot \mathbf{C}]^{\mathrm{sym}} \tag{21}$$

depending on the scalar values $S_i = 2\partial\psi_0/\partial I_i$ and the derivatives of the invariants with respect to the right Cauchy–Green tensor

$$\frac{\partial I_1}{\partial \mathbf{C}} = \mathbf{I}, \quad \frac{\partial I_2}{\partial \mathbf{C}} = \mathbf{C}, \quad \frac{\partial I_3}{\partial \mathbf{C}} = \mathbf{C}^2, \quad \frac{\partial I_4}{\partial \mathbf{C}} = \mathbf{A}, \quad \frac{\partial I_5}{\partial \mathbf{C}} = 2[\mathbf{A} \cdot \mathbf{C}]^{\mathrm{sym}} \tag{22}$$

DOI: 10.1002/nme

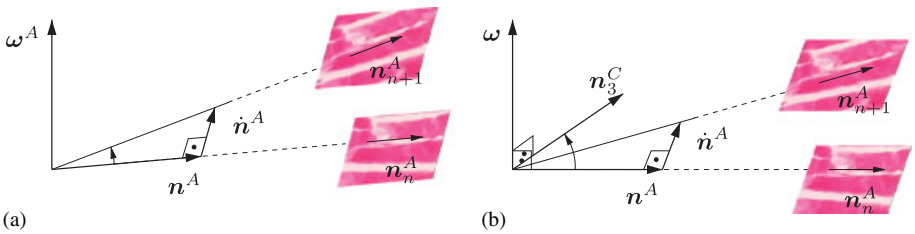

Figure 1. (a) Evolution of characteristic direction amounts to a rotation of the characteristic direction $\mathbf{n}^A$ with the angular velocity $\boldsymbol{\omega}^A$. (b) The characteristic direction $\mathbf{n}^A$ rotates such that in the equilibrium state an alignment with the principal stretch direction $\mathbf{n}^C_3$ is achieved. To avoid drilling rotation, the angular velocity $\boldsymbol{\omega}^A$ must be perpendicular to the plane spanned by $\mathbf{n}^A$ and $\mathbf{n}^C_3$.

From Equation (21), one can easily read that coaxiality of the structural tensor $\mathbf{A}$ and the right Cauchy–Green tensor $\mathbf{C}$ involves coaxiality of the Piola–Kirchhoff stresses $\mathbf{S}$ and the right Cauchy–Green tensor $\mathbf{C}$. Such coaxiality can be achieved by aligning the characteristic direction $\mathbf{n}^A$ with one of the principal directions of the right Cauchy–Green tensor. Hence, in this contribution, we assume an alignment with the maximum principal stretch direction

$$\mathbf{n}^A \rightsquigarrow \mathbf{n}^C_3 \quad \text{for } \lambda^C_1 \leqslant \lambda^C_2 < \lambda^C_3 \tag{23}$$

see also Equations (3) and (4). Such an ansatz is particularly reasonable for the computation of biomaterials and during optimization processes in material or structural design. Analogous to the theory of smooth shells, see for instance, Betsch *et al.* [39] and the references cited therein, we exclude drilling rotations about the characteristic direction $\mathbf{n}^A$. As depicted in Figure 1(b), the angular velocity must be perpendicular to the plane spanned by $\mathbf{n}^A$ and $\mathbf{n}^C_3$, which we incorporate *via*

$$\boldsymbol{\omega}^A := \frac{\pi}{2t^\star}\mathbf{n}^A \times \mathbf{n}^C_3 \tag{24}$$

where the material parameter $t^\star > 0$ acts like a relaxation parameter, see also Menzel [6]. For $t^\star \to \infty$, one can easily observe from Equation (24) that the evolution of the characteristic direction tends to zero $\dot{\mathbf{n}}^A \to \mathbf{0}$, or the characteristic direction remains constant. Moreover, the closer the angle between the two vectors the smaller the values that the norm of their cross product takes. Accordingly, the norm of the angular velocity in Equation (24) takes high values for large differences between $\mathbf{n}^A$ and $\mathbf{n}^C_3$ and low values if the two vectors are almost aligned. The angular velocity is thus assumed to be higher at the beginning of the reorientation process than close to the final equilibrium state at the end of the reorientation process. The same effect can be observed by insertion of Equation (24) into Equation (20)

$$\dot{\mathbf{n}}^A = \frac{\pi}{2t^\star}[\mathbf{I} - \mathbf{n}^A \otimes \mathbf{n}^A] \cdot \mathbf{n}^C_3 \tag{25}$$

The rate of change of the characteristic direction is the part of $\mathbf{n}^C_3$ perpendicular to $\mathbf{n}^A$ weighted by the constant scalar $\pi/(2t^\star)$. Thus, the reorientation occurs proportional to the sinus of the angle between $\mathbf{n}^A$ and $\mathbf{n}^C_3$. The magnitude of the stretch does not, however, have any influence on the reorientation model applied here. For other strain-based formulations of reorientation the reader is referred to Imatani and Maugin [8], Kuhl *et al.* [5] and Driessen *et al.* [1–4], as well as to Driessen *et al.* [40], wherein the applied reorientation model is additionally assumed to depend on the magnitude of the principal stretches.

DOI: 10.1002/nme

Remark 3.1 (*Details on the strain-driven reorientation process*)
Since the material behaviour depends on the orientation but not on the direction of $\mathbf{n}^A$, see Equations (7) and (11), the orientation of the principal stretch direction $\mathbf{n}_3^C$ is changed to $-\mathbf{n}_3^C$, if the angle enclosed with the characteristic direction $\mathbf{n}^A$ is obtuse. For the sake of simplicity, we shall assume that for multiple maximum stretch directions $\lambda_1^C \leqslant \lambda_2^C = \lambda_3^C$, the characteristic direction stays constant, $\dot{\mathbf{n}}^A = \mathbf{0}$, compare Menzel [6].

Remark 3.2 (*Alternative driving forces for the reorientation process*)
For soft tissues it can be shown that a reorientation along principal stress directions is more reasonable, see for instance, Hariton *et al*. [7] and related discussions in Menzel [6]. A stress-based reorientation coupled with volumetric degradation of the material for thermodynamically consistent finite elastoplasticity has been discussed in Johansson *et al*. [18]. For reorientation of microstructures in liquid crystals or piezoelectric materials a formulation driven by gradients of the electric or the magnetic fields seems to be more realistic from a physical point of view.

4. CONSISTENT LINEARIZATION

For the implementation into a finite element program, standard finite elements can be used with an internal variable formulation for the characteristic direction $\mathbf{n}^A$.

4.1. Incremental update of characteristic direction

For the time integration of the evolution equation (20), an implicit Euler backward scheme as discussed in Hughes and Winget [41] is conceivable, i.e. $\mathbf{n}_{n+1}^A = \mathbf{n}_n^A + \dot{\mathbf{n}}_{n+1}^A \Delta t$. For such an update algorithm, a post-processing normalization $\mathbf{n}_{n+1}^A \leftarrow \mathbf{n}_{n+1}^A / \|\mathbf{n}_{n+1}^A\|$ is necessary to ensure that the characteristic direction remains a unit vector.

In this work, however, a geometrically exact update is applied. The infinitesimal version of the Euler theorem indicates that the exponent $\exp(\hat{\boldsymbol{\omega}}^A \Delta t) \in \mathscr{SO}(3)$ of the skew symmetric tensor $\hat{\boldsymbol{\omega}}^A$ is a rotation about its axial vector $\boldsymbol{\omega}^A$ by the angle $(\|\boldsymbol{\omega}^A\| \Delta t)$, see Marsden and Ratiu [42] and Gurtin [43]. Thus, the implicit exponential map

$$\mathbf{n}_{n+1}^A = \exp(\hat{\boldsymbol{\omega}}_{n+1}^A \Delta t) \cdot \mathbf{n}_n^A \tag{26}$$

with the index n denoting the time increment, describes a rotation of the characteristic direction of the last time step $\mathbf{n}_n^A$ about the current axis $\boldsymbol{\omega}_{n+1}^A$. Hence, the characteristic direction in (26) remains a unit vector during the update procedure and a normalization is not necessary. The exponential expression in (26) can be rewritten by the Rodriguez formula

$$\exp(-\boldsymbol{\varepsilon} \cdot \boldsymbol{\omega}^A \Delta t) = \cos(\omega \Delta t)\mathbf{I} + [1 - \cos(\omega \Delta t)]\mathbf{n}^\omega \otimes \mathbf{n}^\omega + \sin(\omega \Delta t)\hat{\mathbf{n}}^\omega \tag{27}$$

see Marsden and Ratiu [42]. Herein, $\omega = \|\boldsymbol{\omega}^A\|$, $\mathbf{n}^\omega = \boldsymbol{\omega}^A / \omega$ and $\hat{\mathbf{n}}^\omega = -\boldsymbol{\varepsilon} \cdot \mathbf{n}^\omega$ are the norm of the angular velocity, the direction of the angular velocity and the corresponding skew symmetric tensor, respectively.

The non-linear residual equation related to (26)

$$\mathbf{r} = -\mathbf{n}_{n+1}^A + \exp(\hat{\boldsymbol{\omega}}_{n+1}^A \Delta t) \cdot \mathbf{n}_n^A = \mathbf{0} \tag{28}$$

DOI: 10.1002/nme

can be solved by a Newton iteration scheme. Hence, Equation (28) is expanded in linear Taylor series at $\mathbf{n}^A$ as

$$\mathbf{r}^{k+1} = \mathbf{r}^k + \nabla_{\mathbf{n}^A}\mathbf{r}^k \cdot \Delta\mathbf{n}^A = \mathbf{0} \tag{29}$$

For the sake of readability the indices $n+1$ and k are neglected in the following. Thus, the combination of Equations (28) and (29) can be rewritten as

$$\mathbf{r}^{k+1} = \mathbf{r} - \Delta\mathbf{n}^A + \frac{\partial(\exp(\hat{\boldsymbol{\omega}}^A\Delta t)\cdot\mathbf{n}_n^A)}{\partial\mathbf{n}^A}\cdot\Delta\mathbf{n}^A = \mathbf{0} \tag{30}$$

and solved for the increment

$$\Delta\mathbf{n}^A = \left[\mathbf{I} - \frac{\partial(\exp(\hat{\boldsymbol{\omega}}^A\Delta t)\cdot\mathbf{n}_n^A)}{\partial\mathbf{n}^A}\right]^{-1}\cdot\mathbf{r} \tag{31}$$

For the derivative of the exponential expression with respect to the characteristic direction, we apply the chain rule

$$\frac{\partial\exp(\hat{\boldsymbol{\omega}}^A\Delta t)}{\partial\mathbf{n}^A} = \frac{\partial\exp(\hat{\boldsymbol{\omega}}^A\Delta t)}{\partial(\boldsymbol{\omega}^A\Delta t)}\Delta t\cdot\frac{\partial\boldsymbol{\omega}^A}{\partial\mathbf{n}^A} \tag{32}$$

wherein the derivative of the exponent of the skew symmetric tensor with respect to the corresponding axial vector can be determined by means of Rodriguez' formula (27) as described in Appendix A. The derivative of the angular velocity with respect to the characteristic vector

$$\frac{\partial\boldsymbol{\omega}^A}{\partial\mathbf{n}^A} = \frac{\pi}{2t^\star}\boldsymbol{\varepsilon}\cdot\mathbf{n}_3^C = -\frac{\pi}{2t^\star}\hat{\mathbf{n}}_3^C \tag{33}$$

follows straightforwardly from the definition of the angular velocity (24).

Reformulation of the evolution equation (20) in an incremental manner yields the increment of the characteristic direction as

$$\Delta\mathbf{n}^A = \Delta\boldsymbol{\omega}^A\times\mathbf{n}^A \tag{34}$$

including the incremental angular velocity $\Delta\boldsymbol{\omega}^A = {\boldsymbol{\omega}^A}_{n+1}^{k+1}\Delta t - {\boldsymbol{\omega}^A}_{n+1}^{k}\Delta t$. Based on this and excluding drilling rotations, the cross-product of $\mathbf{n}^A$ and $\Delta\mathbf{n}^A$

$$\mathbf{n}^A\times\Delta\mathbf{n}^A = \underbrace{[\mathbf{n}^A\cdot\mathbf{n}^A]}_{=1}\Delta\boldsymbol{\omega}^A - \underbrace{[\mathbf{n}^A\cdot\Delta\boldsymbol{\omega}^A]}_{=0}\mathbf{n}^A \tag{35}$$

yields the incremental angular velocity

$$\Delta\boldsymbol{\omega}^A = \mathbf{n}^A\times\Delta\mathbf{n}^A \tag{36}$$

Thus, the updated characteristic direction becomes

$${\mathbf{n}^A}^{k+1} = \exp(\Delta\hat{\boldsymbol{\omega}}^A)\cdot\mathbf{n}^A = \exp(-\boldsymbol{\varepsilon}\cdot[\mathbf{n}^A\times\Delta\mathbf{n}^A])\cdot\mathbf{n}^A \tag{37}$$

see also Betsch *et al.* [39].

DOI: 10.1002/nme

4.2. Incremental tangent modulus

With the characteristic direction and the strains at hand, the stresses can be derived. Based on (13), the relation between the incremental stresses and incremental strains results in

$$\Delta\mathbf{S} = \mathbb{C} : \tfrac{1}{2}\Delta\mathbf{C} \tag{38}$$

with the incremental tangent modulus $\mathbb{C}$ describing the change of stresses with respect to the change of strains

$$\mathbb{C} = 2\frac{\partial\mathbf{S}}{\partial\mathbf{C}} + 2\frac{\partial\mathbf{S}}{\partial\mathbf{n}^A}\cdot\frac{\partial\mathbf{n}^A}{\partial\mathbf{C}} \tag{39}$$

The first part of Equation (39) can be identified as the elastic tangent modulus

$$\mathbb{C}^e = 2\frac{\partial\mathbf{S}}{\partial\mathbf{C}} = 4\frac{\partial^2\psi_0}{\partial\mathbf{C}\,\partial\mathbf{C}} \tag{40}$$

which can alternatively be represented depending on the invariants by application of the chain rule

$$\mathbb{C}^e = 4\sum_{i=1}^{5}\left[\sum_{j=1}^{5}\left[\frac{\partial^2\psi_0}{\partial I_i\,\partial I_j}\frac{\partial I_i}{\partial\mathbf{C}}\otimes\frac{\partial I_j}{\partial\mathbf{C}}\right] + \frac{\partial\psi_0}{\partial I_i}\frac{\partial^2 I_i}{\partial\mathbf{C}\,\partial\mathbf{C}}\right] \tag{41}$$

see Equations (11) and (21). For the second part of Equation (39), we introduce a fourth-order tangent modulus $\mathbb{C}^n$ measuring the sensitivity of the stresses with respect to the structural tensor. By analogy with Equations (40) and (41), we obtain

$$\mathbb{C}^n = 2\frac{\partial\mathbf{S}}{\partial\mathbf{A}} = 4\frac{\partial^2\psi_0}{\partial\mathbf{C}\,\partial\mathbf{A}} = 4\sum_{i=1}^{5}\left[\sum_{j=4}^{5}\left[\frac{\partial^2\psi_0}{\partial I_i\,\partial I_j}\frac{\partial I_i}{\partial\mathbf{C}}\otimes\frac{\partial I_j}{\partial\mathbf{A}}\right]\right] + 4\sum_{i=4}^{5}\left[\frac{\partial\psi_0}{\partial I_i}\frac{\partial^2 I_i}{\partial\mathbf{C}\,\partial\mathbf{A}}\right] \tag{42}$$

wherein the fact that the isotropic invariants $I_{i=1,2,3}$ do not depend on the structural tensor has already been considered. Thus the second part of Equation (39) becomes

$$\frac{\partial\mathbf{S}}{\partial\mathbf{n}^A} = \frac{1}{2}\mathbb{C}^n : \frac{\partial\mathbf{A}}{\partial\mathbf{n}^A} = \mathbb{C}^n\cdot\mathbf{n}^A \tag{43}$$

Since solely the evolution of the characteristic direction is given, but not the characteristic direction itself, the last part of Equation (39) cannot be computed as directly as the others. For the computation of this derivative, we differentiate the residual of $\mathbf{n}^A$ in the exponential update scheme as depicted in Equation (28) with respect to the right Cauchy–Green tensor

$$\frac{\partial\mathbf{r}}{\partial\mathbf{C}} = -\frac{\partial\mathbf{n}^A}{\partial\mathbf{C}} + \frac{\partial(\exp(\hat{\boldsymbol{\omega}}^A\Delta t)\cdot\mathbf{n}_n^A)}{\partial\mathbf{C}} + \left[-\mathbf{I} + \frac{\partial(\exp(\hat{\boldsymbol{\omega}}^A\Delta t)\cdot\mathbf{n}_n^A)}{\partial\mathbf{n}^A}\right]\cdot\frac{\partial\mathbf{n}^A}{\partial\mathbf{C}} = \mathbf{0} \tag{44}$$

Solving this equation for the derivative in demand yields

$$\frac{\partial\mathbf{n}^A}{\partial\mathbf{C}} = \left[\mathbf{I} - \frac{\partial(\exp(\hat{\boldsymbol{\omega}}^A\Delta t)\cdot\mathbf{n}_n^A)}{\partial\mathbf{n}^A}\right]^{-1}\cdot\frac{\partial(\exp(\hat{\boldsymbol{\omega}}^A\,\Delta t)\cdot\mathbf{n}_n^A)}{\partial\mathbf{C}} \tag{45}$$

In this, the inverse is identical to the inverse in Equation (31). Analogous to the derivative of the exponential expression in Equation (32), the derivative of the exponential expression with respect

DOI: 10.1002/nme

to the right Cauchy–Green tensor can be solved by application of the chain rule

$$\frac{\partial \exp(\hat{\boldsymbol{\omega}}^A \Delta t)}{\partial \mathbf{C}} = \frac{\partial \exp(\hat{\boldsymbol{\omega}}^A \Delta t)}{\partial (\boldsymbol{\omega}^A \Delta t)} \Delta t \cdot \frac{\partial \boldsymbol{\omega}^A}{\partial \mathbf{C}} \tag{46}$$

with

$$\frac{\partial \boldsymbol{\omega}^A}{\partial \mathbf{C}} = -\frac{\pi}{2t^\star} (\boldsymbol{\varepsilon} \cdot \mathbf{n}^A) \cdot \frac{\partial \mathbf{n}_3^C}{\partial \mathbf{C}} = \frac{\pi}{2t^\star} \hat{\mathbf{n}}^A \cdot \frac{\partial \mathbf{n}_3^C}{\partial \mathbf{C}} \tag{47}$$

The derivative of the eigenvector $\mathbf{n}_3^C$ with respect to its corresponding tensor $\mathbf{C}$ cannot be computed straightforwardly. Following Mosler and Meschke [44], this contribution is derived from the derivative of the eigenvalue problem of $\mathbf{C}$ and the derivative of the normalization condition of $\mathbf{n}_3^C$ as described in Appendix B. A summary of the complete algorithm is given in Table I.

Table I. Algorithmic update scheme.

History data: internal variable $\mathbf{n}_n^A = [n_{n_1}^A, n_{n_2}^A, n_{n_3}^A]^{\mathrm{t}}$

1. Set initial values

   $\mathbf{n}^A = \mathbf{n}_n^A, \quad \mathbf{A} = \mathbf{n}^A \otimes \mathbf{n}^A, \quad \mathbf{C} = \mathbf{F}^{\mathrm{t}} \cdot \mathbf{F}, \quad \mathbf{S} = 2\frac{\partial \psi_0}{\partial \mathbf{C}}$

2. Compute principal stretch directions and eigenvalues

   $\mathbf{C} = \sum_{I=1}^{3} \lambda_I^C \mathbf{n}_I^C \otimes \mathbf{n}_I^C \quad$ with $\lambda_1^C \leqslant \lambda_2^C \leqslant \lambda_3^C$

   IF $\lambda_2^C = \lambda_3^C$ OR $\mathbf{n}^A \parallel \mathbf{n}_3^C$ THEN

   $\dot{\mathbf{n}}^A = \mathbf{0}$, $\mathbb{C} = 2\frac{\partial \mathbf{S}}{\partial \mathbf{C}}$ EXIT

   ELSE

   IF $\mathbf{n}^A \cdot \mathbf{n}_3^C < 0$ THEN $\mathbf{n}_3^C \mapsto -\mathbf{n}_3^C$

3. Local Newton iteration

   (a) compute residual

   $\mathbf{r} = -\mathbf{n}^A + \exp(\hat{\boldsymbol{\omega}}^A \Delta t) \cdot \mathbf{n}_n^A$

   (b) compute incremental update

   $\Delta \mathbf{n}^A = \left[\mathbf{I} - \frac{\partial (\exp(\hat{\boldsymbol{\omega}}^A \Delta t) \cdot \mathbf{n}_n^A)}{\partial \mathbf{n}^A} \right]^{-1} \cdot \mathbf{r}$

   (c) update

   $\mathbf{n}^A \Leftarrow \exp(-\boldsymbol{\varepsilon} \cdot [\mathbf{n}^A \times \Delta \mathbf{n}^A]) \cdot \mathbf{n}^A$

   $\boldsymbol{\omega}^A = \frac{\pi}{2t^\star} \mathbf{n}^A \times \mathbf{n}_3^C$

   (d) check tolerance

   IF $\|\mathbf{r}\| <$ tol GOTO 4

   ELSE GOTO 3.a

4. Compute moduli

   $\mathbb{C} = \mathbb{C}^e + \mathbb{C}^n : \frac{\partial \mathbf{A}}{\partial \mathbf{n}^A} \cdot \left[\mathbf{I} - \frac{\partial (\exp(\hat{\boldsymbol{\omega}}^A \Delta t) \cdot \mathbf{n}_n^A)}{\partial \mathbf{n}^A} \right]^{-1} \cdot \frac{\partial (\exp(\hat{\boldsymbol{\omega}}^A \Delta t) \cdot \mathbf{n}_n^A)}{\partial \mathbf{C}}$

   with $\mathbb{C}^e = 4\frac{\partial^2 \psi_0}{\partial \mathbf{C} \partial \mathbf{C}}$ and $\mathbb{C}^n = 4\frac{\partial^2 \psi_0}{\partial \mathbf{C} \partial \mathbf{A}}$

DOI: 10.1002/nme

5. NUMERICAL EXAMPLES

In this section, the constitutive specifications described previously will be discussed by means of numerical examples. Therefore, we choose an isotropic Neo-Hooke-type free energy function expanded by a transversely isotropic part

$$\psi_0 = \frac{\lambda}{8}\ln^2 J_3 + \frac{\mu}{2}[J_1 - 3 - \ln J_3] + \frac{\alpha}{2}[I_4 - 1]^2 \tag{48}$$

depending on the principal invariants $J_1 = \operatorname{tr}\mathbf{C} = I_1$ and $J_3 = \det\mathbf{C} = \frac{1}{6}I_1^3 - \frac{1}{2}I_1 I_2 + \frac{1}{3}I_3$, as well as the mixed invariant $I_4 = \operatorname{tr}(\mathbf{C}\cdot\mathbf{A})$, see also Equation (11). Convexity-related issues are not the focus of this work—the reader is referred to the contribution by Schröder and Neff [45] for detailed background information. We consider a simple tension test, a transversely isotropic strip under tension and a cylindrical tube under inside pressure-type loading, comparing a material with a fixed characteristic direction with a material including reorientation of the characteristic direction.

5.1. Simple tension test

To set the stage, the material behaviour will be investigated by a simple tension test, for which the maximum principal stretch direction is prescribed. Therefore, a specimen is stretched to one and a half of its original length, as illustrated in Figure 2 on the left. We compare a material with a fixed characteristic direction perpendicular to the maximum principal stretch direction with a material including reorientation of the characteristic direction. For the reorienting material, the initial characteristic direction is either parallel or perpendicular to the maximum principal stretch direction. The three different cases are depicted in Figure 2 on the right. The material parameters are the elasticity modulus $E = 15.0\,\mathrm{N/mm^2}$ and the Poisson ratio $\nu = 0.3$ related to the Lamé constant $\lambda = 8.654\,\mathrm{N/mm^2}$, and the shear modulus $\mu = 5.769\,\mathrm{N/mm^2}$, as well as the anisotropy parameter $\alpha = 5.0\,\mathrm{N/mm^2}$. The relaxation time parameter $t^\star$ is assumed to be larger than the time step $\Delta t = 1.0 < t^\star$, here we choose $t^\star = 10.0$, $t^\star = 100.0$ and $t^\star = 200.0$.

As one can see in Figure 3(a) for the fixed characteristic direction, the angle between the characteristic direction and the principal stretch direction stays, apparently, constantly at 90°. The stresses do not change during the entire loading process and the normal stresses perpendicular to the loading direction vanish, as expected for a standard elastic material. For reorientation

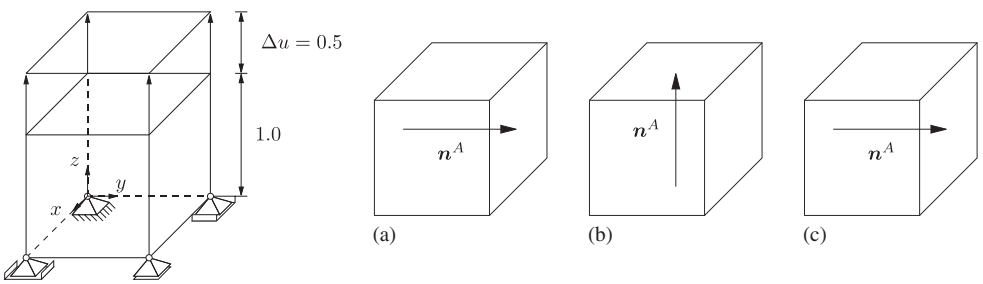

Figure 2. Loads and boundary conditions (left) and orientation of the initial characteristic direction (right) in the simple tension test with (a) $\mathbf{n}^A$ fixed and (b/c) reorientation of $\mathbf{n}^A$.

DOI: 10.1002/nme

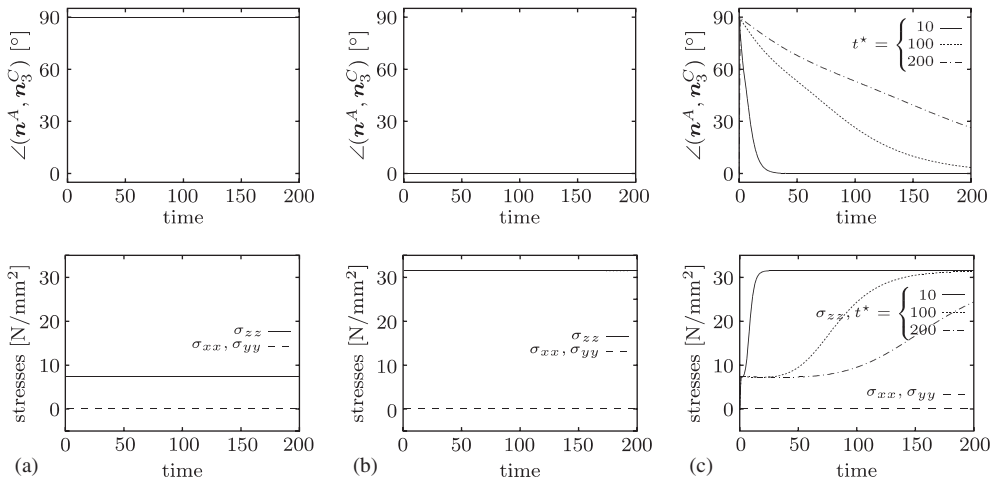

Figure 3. Stresses and angle between the characteristic direction $\mathbf{n}^A$ and principal stretch direction $\mathbf{n}_3^C$ for: (a) $\mathbf{n}^A \perp \mathbf{n}_3^C$, $\mathbf{n}^A$ fixed; (b) $\mathbf{n}^A \parallel \mathbf{n}_3^C$, reorientation; and (c) $\mathbf{n}^A \perp \mathbf{n}_3^C$, reorientation.

with the initial characteristic direction parallel to the maximum principal stretch direction, (see Figure 3(b)), the characteristic direction also stays constant, because the characteristic direction and the maximum principal stretch direction are aligned *ab initio*. Consequently, the stress σ_{zz} is constant, too, but due to the stiffer characteristic direction at a higher level than in Figure 3(a). Finally, for reorientation with the initial characteristic direction perpendicular to the maximum principal stretch direction, one can read from Figure 3(c) that the characteristic direction reorients gradually until it is aligned with the maximum principal stretch direction. As described in Section 3.2, it is observable that the reorientation process proceeds faster at the beginning than close to the final equilibrium state. For higher values of $t^\star$ the relaxation time is longer than for lower values of $t^\star$. As mentioned before for $t^\star \to \infty$ the evolution tends to zero, thus the fibre direction does not change. Furthermore, the normal stress in the loading direction starts with the same value as in Figure 3(a) and changes due to the reorientation and alignment of the stiffer characteristic direction with the loading direction until, in the final equilibrium state, the stresses are equal to that in Figure 3(b).

5.2. Strip under tension

A transversely isotropic strip either with fixed characteristic direction or including reorientation of the characteristic direction is considered under constant displacement load $\Delta u = 1.0$ as depicted in Figure 4. The angle between the initial characteristic direction and vertical axis is assumed to be 45°. For the material parameters we choose $E = 3.0\,\mathrm{N/mm^2}$ and $\nu = 0.3$ related to $\lambda = 1.7314\,\mathrm{N/mm^2}$ and $\mu = 1.154\,\mathrm{N/mm^2}$, as well as the anisotropy parameter $\alpha = 10.0\,\mathrm{N/mm^2}$, and for reorientation the relaxation time parameter $t^\star = 10.0$. The time step is set to $\Delta t = 0.1$. In Figure 5, the deformation and the characteristic direction $\mathbf{n}^A$ in the material configuration are depicted for several time steps. Since the initial characteristic direction coincides for both materials, the deformations for the first loading step are identical in both cases. As expected for transverse isotropy, due to the stiffer characteristic direction, the strip deforms to an s-shape. For the fixed characteristic direction in Figure 5(a), the deformation does not change under the constant displacement load. For the second

DOI: 10.1002/nme

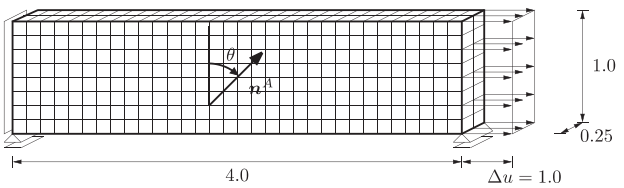

Figure 4. Discretization, loads and boundary conditions of the transversely isotropic strip. A displacement load of $\Delta u = 1.0$ is applied to the left edge. The angle between the initial characteristic direction and the maximum principal stretch direction is denoted by θ.

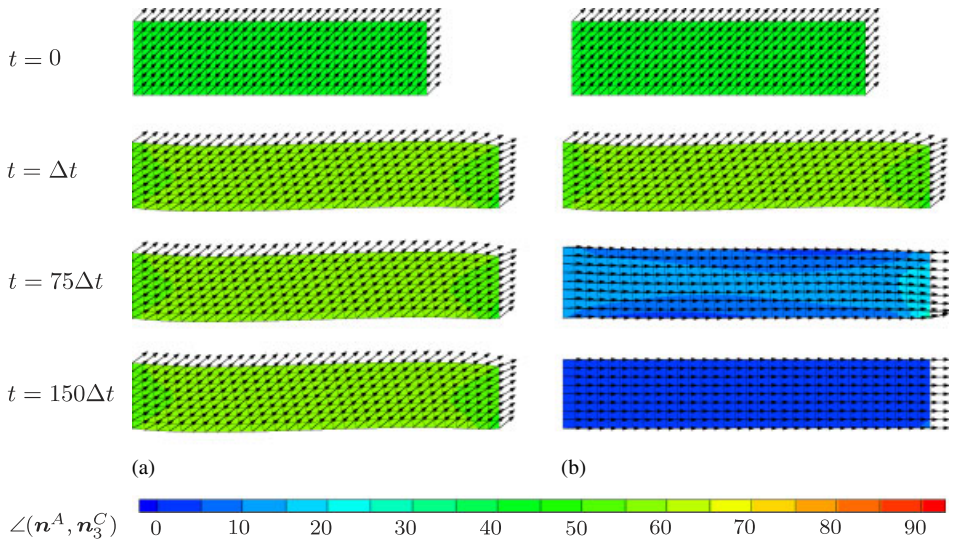

Figure 5. Transversely isotropic strip under tension. The angle between the initial fibre direction and the vertical axis is $\theta = -45°$. Comparison of (a) fixed characteristic direction and (b) reorientation.

case as depicted in Figure 5(b), the characteristic directions rotate until, in the final equilibrium state, the angle between the characteristic direction and the maximum principal stretch direction is zero. Consequently, the deformation of the strip changes from the s-shape to an almost homogeneous elongation of the strip.

Moreover, the computation converges quadratically both on the global and on the local level, as exemplarily depicted in Table II. The left table shows the global convergence for the first three loading steps. In the right table the local convergence in a point of the left bearing is depicted for the four global iterations marked grey in the left table. In the other loading steps, a similar convergence can be observed.

To show the independence of the final state on the initial fibre direction, we additionally study a fibre orientation according to the angle $\theta = -30°$. Further, as described in Remark 3.1, the material behaviour depends only on the orientation of $\mathbf{n}^A$, but not on the direction. To verify this, an initial fibre angle of $\theta = 150°$ is considered so that the fibre points opposite to the direction represented by $\theta = -30°$. As one can see in Figure 6, both the independence on the initial configuration and the independence on the direction of the fibre vector are guaranteed.

DOI: 10.1002/nme

Table II. Quadratic convergence on the global and on the local level.

Global convergence			Local convergence			
Inc	Global it.	Global residual	Inc	Global it.	Local it.	Global residual
1	0	5.19615E+00	1	4	1	1.25502160E−02
1	1	1.76210E−01	1	4	2	3.23125787E−07
1	2	7.68834E−03	1	4	3	1.11022303E−16
1	3	1.42211E−04	1	5	1	1.25502160E−02
1	4	3.46068E−08	1	5	2	3.23125790E−07
1	5	1.59632E−14	1	5	3	1.11022302E−16
2	0	4.24187E−02	2	0	1	1.24318177E−02
2	1	2.85094E−04	2	0	2	3.13964952E−07
2	2	1.63652E−07	2	0	3	1.11022302E−16
2	3	5.42645E−14	2	1	1	1.24644729E−02
3	0	4.22067E−02	2	1	2	3.16473606E−07
3	1	2.81362E−04	2	1	3	1.35525272E−20
3	2	1.52259E−07				
3	3	4.88088E−14				

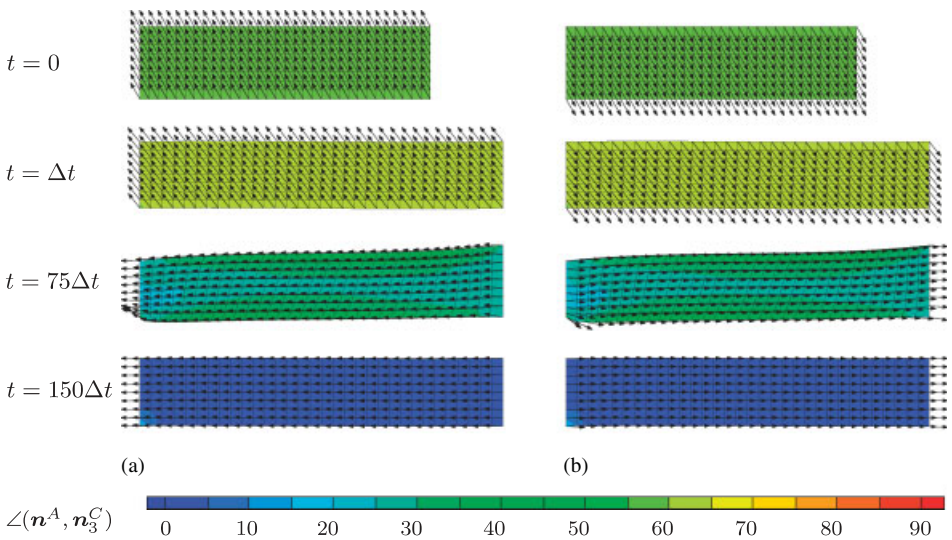

Figure 6. Transversely isotropic strip under tension. The angle between the initial fibre direction and the vertical axis is: (a) $\theta = -30°$ and (b) $\theta = 150°$.

5.3. Tube under inside radial displacement load

In the previous examples, we considered problems with more or less homogeneous deformations in the final state. At this point, we consider a non-homogeneous deformation by means of a transversely isotropic tube with a radial displacement load as depicted in Figure 7. We apply an outwarded sinusoidal displacement load at the inside of the tube with a maximum displacement $u_r^{\max} = 0.3$ in the middle of the tube. The upper and lower boundaries of the tube are

DOI: 10.1002/nme

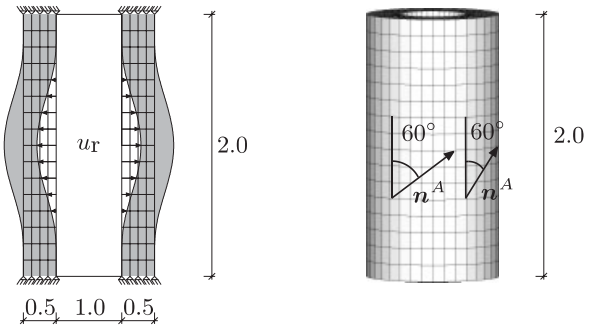

Figure 7. Discretization, loads and boundary conditions of the transversely isotropic tube. A constant sinusoidal displacement load is applied in radial direction at the inside of the tube, with a maximum displacement $u_r^{\max} = 0.3$ in the middle of the tube. The upper and lower boundaries of the tube are completely fixed. The inclination angle of the characteristic direction is 60°.

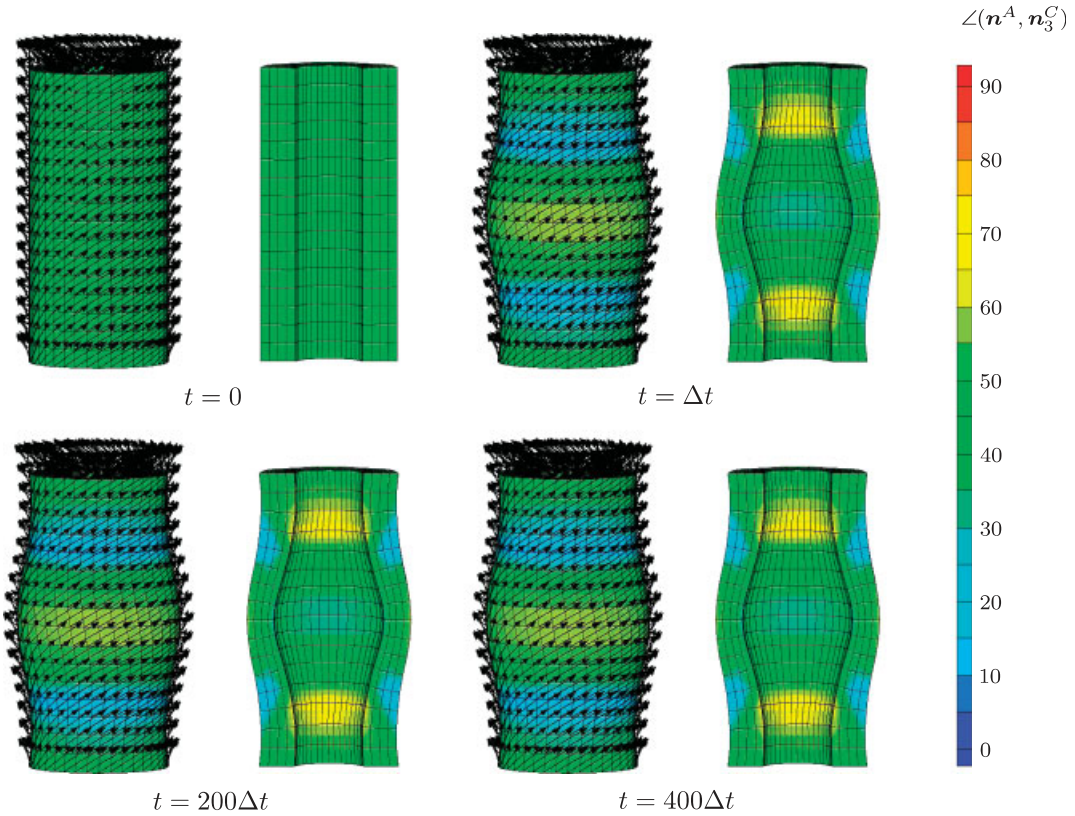

Figure 8. Transversely isotropic tube with fixed characteristic direction. The inclined stiffer fibres cause twisting of the tube. The deformation stays constant for a constant displacement load.

DOI: 10.1002/nme

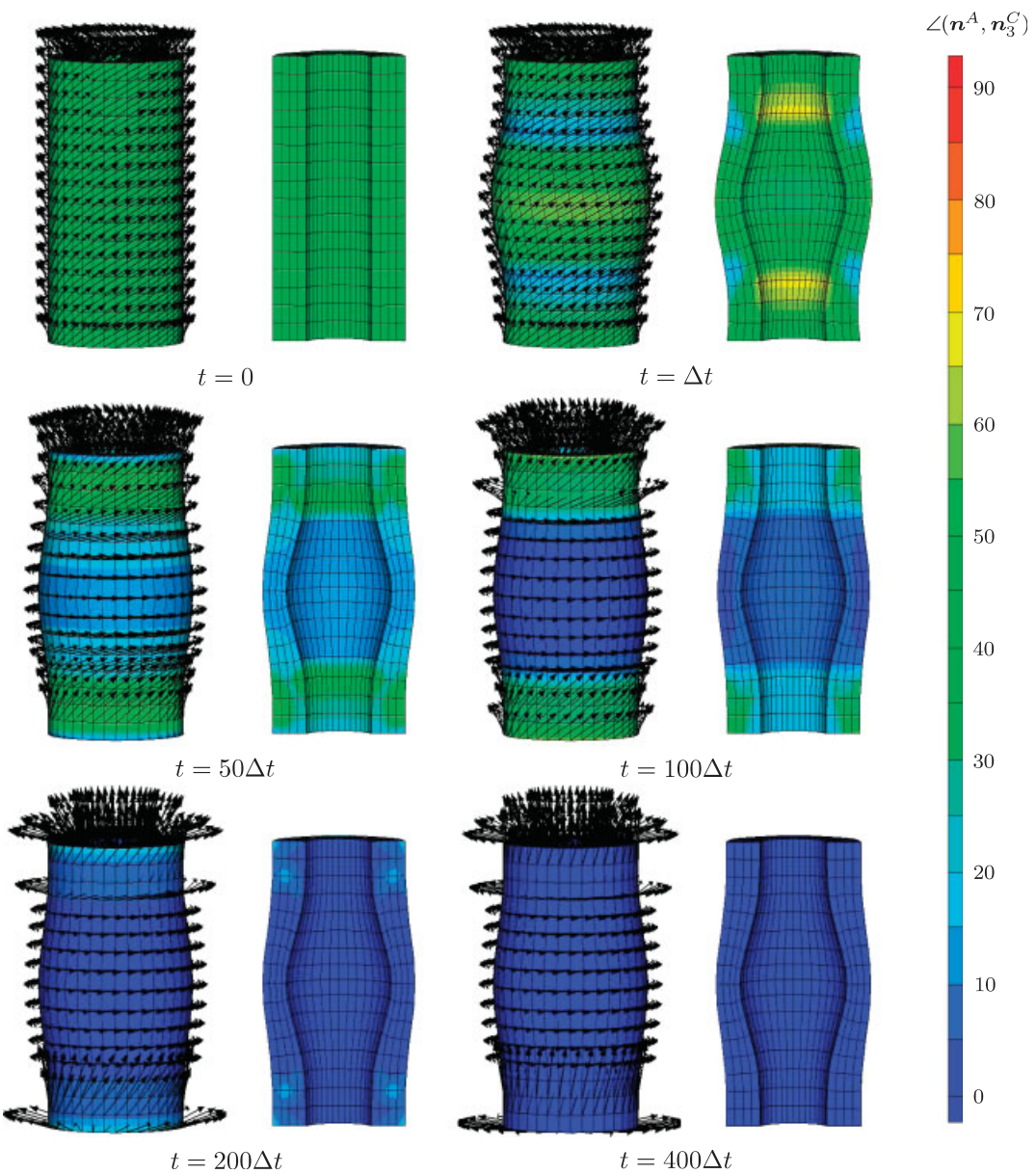

Figure 9. Transversely isotropic tube with fibre reorientation. In the first step, the inclined fibres cause twisting of the tube. The fibres reorient along the maximum principal stretch directions. The reorientation process occurs faster at the begining than towards the final equilibrium state.

fixed in space. The characteristic direction is arranged in the tangential plane with an inclination angle of 60°. The material parameters are $E = 3.0\,\mathrm{N/mm^2}$ and $\nu = 0.4$, related to $\lambda = 4.285\,\mathrm{N/mm^2}$ and $\mu = 1.071\,\mathrm{N/mm^2}$, as well as $\alpha = 2.0\,\mathrm{N/mm}$ and for reorientation $t^\star = 10.0$. The time step is set to $\Delta t = 0.1$. Once more, fixed characteristic directions are compared with reorientation results.

DOI: 10.1002/nme

As one can see in Figure 8, for fixed fibres, the tube twists at the first time step due to higher stiffness of the fibres. The angle between the characteristic direction and the maximum principal stretch direction is distributed inhomogeneously. According to expectations, for a fixed load level, the characteristic direction as well as the deformation stay constant. In Figure 9, the deformation and the fibre directions for reorientation are depicted. For the first time step, as expected, the deformation and fibre distribution is similar to the case with fixed fibres. For the following time steps, however, the fibres begin to rotate until they are aligned with the maximum principal stretch direction. Again, the reorientation proceeds faster at the beginning than close to the final equilibrium state. The maximum principal stretch direction is tangential in the middle of the tube and axial at the upper and lower boundary of the tube. As one can see in Figure 9 for 400 time steps, the final fibre distribution is aligned with the principal stretch direction, which is directed axially in the upper and lower parts and tangentially in the middle part. Apparent non-symmetries occur due to the fact that solely the orientation and not the direction governs the material behaviour. The twist of the tube, indicated at the beginning of the deformation, recedes due to the reorientation of the fibres.

6. CONCLUSION

The main concern of this contribution is the numerical implementation of fibre reorientation processes. For anisotropic elasticity, the free energy reaches a critical state for coaxial stresses and strains. For transverse isotropy such a coaxiality can be achieved if the structural tensor and the strain tensor are coaxial. Accordingly, we postulate a reorientation of fibres along the maximum principal stretch directions. The incorporation of other criteria, such as for instance, reorientation along principal stresses or averaged directions, is straightforward and would require only minor modifications of the numerical treatment. Since related algorithms and issues of implementation follow by analogy for those cases, here we focused exclusively on the strain-driven reorientation. The implementation has been realized by an implicit exponential map for the characteristic direction and application of the Rodriguez formula. Consistent linearizations have been demonstrated on the local reorientation level as well as on the global finite element level. The theory has been discussed by numerical examples. After a demonstration of the general material behaviour in terms of a simple tension test, a deformation with a homogeneous as well as an inhomogeneous final state has been considered within a finite element setting, wherein we compared materials with fixed and reorienting fibre directions. In contrast to existing explicit remodelling algorithms suggested in the literature, the formulation proposed in this contribution is particularly efficient and robust since it relies on consistent algorithmic linearizations both on the local and on the global level. Moreover, the suggested computational scheme will not only be useful for the modelling of biological tissue adaptation but rather can also be applied for applications in the wide field of optimization processes in material and structural designs.

APPENDIX A: DERIVATIVE OF THE EXPONENT OF A SKEW SYMMETRIC TENSOR

The derivative of the exponent of a skew symmetric tensor $\hat{\mathbf{v}}$ can be determined by application of the Rodriguez formula

$$\exp(\hat{\mathbf{v}}) = \cos(v)\mathbf{I} + [1 - \cos(v)]\mathbf{n} \otimes \mathbf{n} + \sin(v)\hat{\mathbf{n}} \tag{A1}$$

DOI: 10.1002/nme

with the norm $v = \|\mathbf{v}\|$, and the normal vector $\mathbf{n} = \mathbf{v}/\|\mathbf{v}\|$ of the axial vector $\mathbf{v} = -\frac{1}{2}\hat{\mathbf{v}}^A : \boldsymbol{\varepsilon}$, as well as the corresponding skew symmetric tensor $\hat{\mathbf{n}} = -\boldsymbol{\varepsilon} \cdot \mathbf{n}$. Based on this and by making use of index notation, the derivative of the exponent of a skew symmetric tensor with respect to the corresponding axial vector is

$$\frac{\partial \exp(\hat{v}_{ij})}{\partial v_k} = -\sin(v)\delta_{ij}n_k + \frac{1-\cos(v)}{v}[\delta_{ik}n_j + \delta_{jk}n_i] - \frac{\sin(v)}{v}\varepsilon_{ijk} + \left[\sin(v) - 2\frac{1-\cos(v)}{v}\right] n_i n_j n_k + \left[\frac{\sin(v)}{v} - \cos(v)\right] \varepsilon_{ijl} n_l n_k \tag{A2}$$

Since this derivative includes terms depending on the inverse of the norm of the axial vector, the limit must be determined by means of l'Hospital's rule when the norm of the axial vector tends to zero

$$\lim_{v \to 0} \frac{\partial \exp(\hat{v}_{ij})}{\partial v_k} = -\varepsilon_{ijk} \tag{A3}$$

APPENDIX B: DERIVATIVE OF THE EIGENVECTOR WITH RESPECT TO THE CORRESPONDING TENSOR

The eigenvalue problem of the symmetric second-order tensor $\mathbf{C} \in \mathbb{R}^{3\times 3}$

$$[\mathbf{C} - \lambda^C \mathbf{I}] \cdot \mathbf{n}^C = \mathbf{0} \tag{B1}$$

yields the eigenvalues $\lambda^C_{I=1,2,3} \in \mathbb{R}$ and the eigenvectors $\mathbf{n}^C_{I=1,2,3} \in \mathbb{R}^3$ of $\mathbf{C}$. To obtain the derivative of the eigenvector $\mathbf{n}^C_I$ with respect to the tensor $\mathbf{C}$ itself, we follow the lines of derivation highlighted in Mosler and Meschke [44] and combine the derivative of the eigenvalue problem (B1) with respect to the individual component $C_{\alpha\beta}$

$$\left[\frac{\partial \mathbf{C}}{\partial C_{\alpha\beta}} - \frac{\partial \lambda^C_I}{\partial C_{\alpha\beta}}\mathbf{I}\right] \cdot \mathbf{n}^C_I + [\mathbf{C} - \lambda^C_I \mathbf{I}] \cdot \frac{\partial \mathbf{n}^C_I}{\partial C_{\alpha\beta}} = \mathbf{0} \tag{B2}$$

with the derivative of the constraint that $\mathbf{n}^C_I$ is a normal vector with respect to $C_{\alpha\beta}$

$$\mathbf{n}^C_I \cdot \mathbf{n}^C_I = 1 \;\Rightarrow\; \mathbf{n}^C_I \cdot \frac{\partial \mathbf{n}^C_I}{\partial C_{\alpha\beta}} = 0 \tag{B3}$$

in a linear system of equations

$$\underbrace{\begin{bmatrix} \mathbf{C} - \lambda^C_I \mathbf{I} & -\mathbf{n}^C_I \\ \mathbf{n}^{C\mathrm{t}}_I & 0 \end{bmatrix}}_{\mathbf{K}} \cdot \begin{bmatrix} \dfrac{\partial \mathbf{n}^C_I}{\partial C_{\alpha\beta}} \\ \dfrac{\partial \lambda^C_I}{\partial C_{\alpha\beta}} \end{bmatrix} = \begin{bmatrix} -\dfrac{\partial \mathbf{C}}{\partial C_{\alpha\beta}} \cdot \mathbf{n}^C_I \\ 0 \end{bmatrix} \tag{B4}$$

The derivative of the eigenvector with respect to one individual component $C_{\alpha\beta}$ can be obtained by solving this linear system of Equations (B4) for the vector $[[\partial \mathbf{n}^C_I / \partial C_{\alpha\beta}]^{\mathrm{t}}, \partial \lambda^C_I / \partial C_{\alpha\beta}]^{\mathrm{t}}$, for instance,

DOI: 10.1002/nme

by inverting $\mathbf{K}$. Application of this procedure to each component of the tensor $\mathbf{C}$ generates nine vectors $\partial \mathbf{n}_I^C / \partial C_{\alpha\beta} \in \mathbb{R}^3$, which can be combined in the quantity $\partial \mathbf{n}_I^C / \partial \mathbf{C} \in \mathbb{R}^{3\times3\times3}$.

For identical eigenvalues λ_I^C of $\mathbf{C}$ the matrix $\mathbf{K}$ becomes singular. In that case, small perturbations $\delta \ll 1$ can be applied to the eigenvalues

$$\text{IF} \quad \frac{|\lambda_A - \lambda_B|}{\max(|\lambda_A|, |\lambda_B|, |\lambda_C|)} < \text{tol}_\delta \quad \text{THEN} \begin{cases} \lambda_A = \lambda_A[1+\delta] \\ \lambda_B = \lambda_B[1-\delta] \\ \lambda_C = \lambda_C/[[1+\delta][1-\delta]] \end{cases} \tag{B5}$$

See, for instance, Miehe [46].

REFERENCES

1. Driessen JBN, Boerboom RA, Huyghe JM, Bouten CVC, Baaijens FPT. Computational analyses of mechanically induced collagen fiber remodeling in the aortic heart valve. *Journal of Biomechanical Engineering* 2003; **125**: 549–557.
2. Driessen NJB, Bouten CVC, Baaijens FPT. Improved prediction of the collagen fiber architecture in the aortic heart valve. *Journal of Biomechanical Engineering* 2005; **127**:329–336.
3. Driessen NJB, Peters GWM, Huyghe JM, Bouten CVC, Baaijens FPT. Remodelling of continuously distributed collagen fibres in soft connective tissues. *Journal of Biomechanics* 2003; **36**:1151–1158.
4. Driessen NJB, Wilson W, Bouten CVC, Baaijens FPT. A computational model for collagen fibre remodelling in the arterial wall. *Journal of Theoretical Biology* 2004; **226**:53–64.
5. Kuhl E, Garikipati K, Arruda EM, Grosh K. Remodeling of biological tissue: mechanically induced reorientation of a transversely isotropic chain network. *Journal of the Mechanics and Physics of Solids* 2005; **53**:1552–1573.
6. Menzel A. Modelling of anisotropic growth in biological tissues—a new approach and computational aspects. *Biomechanics and Modeling in Mechanobiology* 2005; **3**(3):147–171.
7. Hariton I, deBotton G, Gasser TC, Holzapfel GA. Stress-driven collagen fiber remodeling in arterial walls. *Biomechanics and Modeling in Mechanobiology* 2007; **6**(3):163–175.
8. Imatani S, Maugin GA. A constitutive model for material growth and its application to three-dimensional finite element analysis. *Mechanics Research Communications* 2002; **29**:477–483.
9. Menzel A. Anisotropic remodelling of biological tissues. In *Mechanics of Biological Tissue*, Holzapfel GA, Ogden RW (eds); *IUTAM Symposium*. Springer: Berlin, 2006; 91–104.
10. Collings PJ. *Liquid Crystals*: *Nature's Delicate Phase of Matter*. Princeton University Press: Princeton, NJ, 1990.
11. Ericksen JL. *Introduction to the Thermodynamics of Solids* (1st edn). Chapman & Hall: London, 1991; 128–150.
12. Kamlah M. Ferroelectric and ferroelastic piezoceramics—modeling of electromechanical hysteresis phenomena. *Continuum Mechanics and Thermodynamics* 2001; **13**:219–268.
13. Smith RC. *Smart Material Systems*. SIAM: Philadelphia, PA, 2005.
14. Schröder J, Romanowski H. A thermodynamically consistent mesoscopic model for transversely isotropic ferroelectric ceramics in a coordinate-invariant setting. *Archive of Applied Mechanics* 2005; **74**:863–877.
15. Arockiarajan A, Delibas B, Menzel A, Seemann W. Studies on rate-dependent switching effects of piezoelectric materials using a finite element model. *Computational Materials Science* 2006; **37**:306–317.
16. Arockiarajan A, Menzel A, Delibas B, Seemann W. Computational modeling of rate-dependent domain switching in piezoelectric materials. *European Journal of Mechanics–A/Solids* 2006; **25**(6):950–964.
17. Arockiarajan A, Menzel A, Delibas B, Seemann W. Micromechanical modeling of switching effects in piezoelectric materials—a robust coupled finite element approach. *Journal of Intelligent Material Systems and Structures* 2006. DOI 10.1177/1045389x06074117
18. Johansson G, Menzel A, Runesson K. Modeling of anisotropic inelasticity in pearlitic steel at large strains due to deformation induced substructure evolution. *European Journal of Mechanics–A/Solids* 2005; **24**(6):899–918.
19. Kocks UF, Tomé CN, Wenk H-R (eds). *Texture and Anisotropy—Preferred Orientations in Polycrystals and their Effect on Material Properties*. Cambridge University Press: Cambridge, 2000.
20. Pedersen NL. On design of fiber-nets and orientation for eigenfrequency optimization of plates. *Computational Mechanics* 2006; **39**(1):1–13.

DOI: 10.1002/nme

21. Vianello M. Coaxiality of strain and stress in anisotropic linear elasticity. *Journal of Elasticity* 1996; **42**:283–289.
22. Vianello M. Optimization of the stored energy and coaxiality of strain and stress in finite elasticity. *Journal of Elasticity* 1996; **44**:193–202.
23. Sgarra C, Vianello M. Directions of coaxiality between pure strain and stress in linear elasticicty. *Journal of Elasticity* 1997; **46**:263–265.
24. Chadwick P. *Continuum Mechanics. Concise Theory and Problems*. Allen & Unwin Ltd: London, 1976.
25. Holzapfel GA. *Nonlinear Solid Mechanics*, *A Continuum Approach for Engineering*. Wiley: New York, 2000.
26. Borchardt-Ott W. *Kristallographie*. Springer: Berlin, 1997.
27. Lokhin VV, Sedov LI. Nonlinear tensor functions of several tensor arguments. *Journal of Applied Mathematics and Mechanics* 1963; **27**(3):393–417.
28. Boehler JP. A simple derivation of representations for non-polynomial constitutive equations in some cases of anisotropy. *Zeitschrift für Angewandte Mathematik und Mechanik* 1979; **59**:157–167.
29. Spencer AJM. Theory of invariants. In *Continuum Physics*, Eringen C (ed.), vol. 1. Academic Press: New York, 1971.
30. Schröder J. Theoretische und algorithmische Konzepte zur phänomenologischen Beschreibung anisotropen Materialverhaltens. *Ph.D. Thesis*, Institut für Mechanik und Numerische Mechanik, Universität Hannover, Hannover, 1996.
31. Garikipati K, Olberding JE, Narayanan H, Arruda EM, Grosh K, Calve S. Biological remodelling: stationary energy, configurational change, internal variables and dissipation. *Journal of the Mechanics and Physics of Solids* 2006; **54**:1493–1515.
32. Epstein M, Maugin GA. Thermomechanics of volumetric growth in uniform bodies. *International Journal of Plasticity* 2000; **16**:951–978.
33. Kuhl E, Steinmann P. On spatial and material settings of thermo-hyperelastodynamics for open systems. *Acta Mechanica* 2003; **160**:179–217.
34. Kuhl E, Steinmann P. Theory and numerics of geometrically nonlinear open system mechanics. *International Journal for Numerical Methods in Engineering* 2003; **58**:1593–1615.
35. Himpel G. *On the Modeling of Material Growth in Anisotropic Solids. Internal Variable Approach and Numerical Implementation*. Diplomarbeit, Institut für Mechanik (Bauwesen), Lehrstuhl I, Universität Stuttgart, 2003.
36. Menzel A, Steinmann P. A view on anisotropic finite hyperelasticity. *European Journal of Mechanics – A/Solids* 2003; **22**(1):71–87.
37. Cowin SC. Optimization of the strain energy density in linear anisotropic elasticity. *Journal of Elasticity* 1994; **34**:45–68.
38. Sgarra C, Vianello M. Rotations which make strain and stress coaxial. *Journal of Elasticity* 1997; **47**:217–224.
39. Betsch P, Menzel A, Stein E. On the parametrisation of finite rotations in computational mechanics—a classification of concepts with application to smooth shells. *Computer Methods in Applied Mechanics and Engineering* 1998; **155**:273–305.
40. Driessen NJB, Cox MAJ, Bouten CVC, Baaijens FPT. Remodelling of the angular collagen fiber distribution in cardiovascular tissues. *Biomechanics and Modeling in Mechanobiology* 2007. DOI 10.1007/s10237-007-0078-x
41. Hughes TJR, Winget J. Finite rotation effects in numerical integration of rate constitutive equations arising in large-deformation analysis. *International Journal for Numerical Methods in Engineering* 1980; **15**:1862–1867.
42. Marsden JE, Ratiu TS. *Introduction to Mechanics and Symmetry*. Springer: Berlin, 1994.
43. Gurtin ME. *An Introduction to Continuum Mechanics. Mathematics in Science and Engineering*, vol. 158. Academic Press: New York, 1981.
44. Mosler J, Meschke G. 3D modeling of strong discontinuities in elastoplastic solids: fixed and rotating localization formulations. *International Journal for Numerical Methods in Engineering* 2003; **57**:1553–1576.
45. Schröder J, Neff P. Invariant formulation of hyperelastic transverse isotropy based on polyconvex free energy functions. *International Journal of Solids and Structures* 2003; **40**:401–445.
46. Miehe C. Computation of isotropic tensor functions. *Communications in Numerical Methods in Engineering* 1993; **9**(11):889–896.

DOI: 10.1002/nme